Building and Environment 194 (2021) 107650

Contents lists available at ScienceDirect

Building and Environment

journal homepage: www.elsevier.com/locate/buildenv

Separate and combined impacts of building and tree on urban thermal environment from two- and three-dimensional perspectives

Jike Chen [a], Wenfeng Zhan [b,c], Shuangen Jin [a,g,*], Wenquan Han [d], Peijun Du [e], Junshi Xia [f], Jiameng Lai [b,c], Jiufeng Li [b,c], Zihan Liu [b,c], Long Li [b,c], Fan Huang [b,c], Haiyong Ding [a]

[a] School of Remote Sensing & Geomatics Engineering, Nanjing University of Information Science & Technology, Nanjing 210044, China
[b] Jiangsu Provincial Key Laboratory of Geographic Information Science and Technology, International Institute for Earth System Science, Nanjing University, Nanjing 210023, China
[c] Jiangsu Center for Collaborative Innovation in Geographical Information Resource Development and Application, Nanjing, 210023, China
[d] Nanjing Institute of Surveying, Mapping & Geotechnical Investigation, Co. Ltd Nanjing 210019, China
[e] Key Laboratory for Land Satellite Remote Sensing Applications of Ministry of Natural Resources, Nanjing University, Nanjing 210093, China
[f] RIKEN Center for Advanced Intelligence Project, RIKEN, Tokyo 103-0027, Japan
[g] Shanghai Astronomical Observatory, Chinese Academy of Science, Shanghai 200030, China

ARTICLE INFO

Keywords:
Land surface temperature
Building
Tree
Landscape pattern
Multi-dimensional characteristics

ABSTRACT

Separate impacts of building and tree on the urban thermal environment have been studied extensively, but their combined impacts, especially from both the horizontal (i.e., two-dimensional (2D)) and vertical (i.e., three-dimensional (3D)) perspectives remain largely unclear. Based on satellite thermal data and elaborate 2D and 3D urban morphology, herein we simultaneously investigate the separate and combined impacts of building and tree over Nanjing in China from both the 2D and 3D perspectives. We further examine the day–night contrast together with the sensitivity of such impacts to scale. Our results show that, when compared with urban structures from a single dimension, the combination of 2D and 3D structures is more capable of predicting urban land surface temperatures (LSTs) for both day and night. The assessments further illustrate that the separate and combined impacts of building and tree on LSTs are usually more significant when the spatial scale increases. As for the separate impacts of building and tree, 2D structure affects more urban thermal environment than 3D structure at all spatial scales during the day, but an opposite trend occurs at night. Moreover, for the combined impact of building and tree on LST across different scales, daytime and nighttime LSTs are respectively dominated by 2D and 3D building structures. Combining 2D and 3D structures improves the explained LST variation by 7.3%–11.1% and 25.3%–37.7% for day and night, respectively when compared to using 2D structures only. These findings emphasize the need to incorporate both 2D and 3D urban morphology to improve the urban thermal environment.

1. Introduction

Urbanization is a complex process characterized by the transition of natural landscape into impervious surfaces [1,2]. One of the most phenomenal effects of this landscape transition is the urban heat island (UHI) [3]. UHI is able to increase the consumption of energy and water as well as exert a great threat to public health, and it has been therefore investigated over global cities [4–6]. Recent decades has been witnessing an increasing amount of studies on surface UHI (SUHI) with remote sensing [7–11], mostly because of the wide availability of satellite-derived land surface temperature (LST) data acquired from various satellite sensors (e.g., Advanced Spaceborne Thermal Emission and Reflection Radiometer (ASTER) [12] and Landsat Thematic Mapper (TM) [13]). In addition to thermal data, satellite remote sensing further facilitates the investigation of SUHI by obtaining detailed information on urban fabrics and geometry (e.g., on buildings and trees) with high-resolution visible and near-infrared images [14,15].

SUHI (or LST) is closely associated with urban morphology from both the two-dimensional (2D) and three-dimensional (3D) perspectives [16]. From the 2D perspective, previous concerns have been concentrating on the relationships between SUHI (or LST) and landscape pattern (including composition and configuration [17], especially for building and tree [18,19]. Previous studies have demonstrated that the effect of the spatial configuration of building and tree on LST varied

* Correspondence to: Nanjing University of Information Science & Technology, No. 219 Ningliu Road, Pukou District, Nanjing, 210044, China.
E-mail address: sgjin@nuist.edu.cn (S. Jin).

https://doi.org/10.1016/j.buildenv.2021.107650
Received 10 July 2020; Received in revised form 25 December 2020; Accepted 24 January 2021
Available online 13 February 2021

with position, orientation, and arrangement [18], and their in-between relationships demonstrated a day–night contrast [18,20].

It is further suggested that the relationships between LST and the 2D landscape pattern are scale-dependent [21]. A single scale of analysis is always arbitrary, and thus generates mismatching results between researches [22]. Investigation of the relationship between LST and landscape pattern was therefore recommended at different scales simultaneously (i.e., statistical units of varying size) [23]. For instance, among various scales, the unit sizes of 660 and 720 m were found the most appropriate to examine the sensitivity of the relationship between LST and landscape composition [24]. This may be explained by the fact the interactions and exchanges across land cover patches exerted the most important influences on the heat exchange at these scales [25]. In addition, current studies indicated that different influencing factors may reflect ecological processes at different scales, and thus their relative importances controlling urban thermal environment appear to vary with the spatial scale [25,26].

Considering that 3D urban morphology can regulate urban thermal environment by affecting air circulation, solar radiation and evapotranspiration within urban canyons [27–29], a few studies emerged recently to explore the control of urban morphology on LST from the 3D perspective. Studies have illustrated that there existed a strong relationship between vegetation height and LST, and LST decreased at an increasing rate with vegetation height [30]. Similar to the 2D perspective case, the relationships between LST and vertical tree structure during the day differed from those at night [31]. Regardless of different seasons, the taller the height of buildings are, the cooler urban thermal environment is during the day [32].

Some recent studies attempted to investigate the impacts of building and tree on UHI from both 2D and 3D perspectives, and found that combining 2D and 3D urban morphology could better explain LST variations. However, there is a difference in relative importance between 2D and 3D building indicators towards regulating LST. LST was observed more dependent on the 3D than 2D building indicators in Yazd, Iran [33], while an opposite trend occurred in Wuhan, China [34]. Indicators such as building height, percent cover of building, and 3D spatial orientation of buildings were found to be the strongest controls among all the 2D and 3D building indicators [33,35].

Building and tree are mostly mutually inclusive over urban landscape. While the separate impacts of building and tree on local thermal environment have been analyzed, their combined impacts of building and tree from both the 2D and 3D perspectives remain largely unclear. Urban thermal environment responsive to urban morphology is scale-dependent, but as far as we know, there is still no attempt on how the impacts on LST vary with scale from both the 2D and 3D perspectives. This initiates an urgent need to understand the interactions between the local thermal environment and building and tree at multiple spatial scales from both the 2D and 3D perspectives. Here, we try to address the following issues: (1) To what extent the combination of 2D and 3D urban morphology will improve the explanatory power of LST variation, compared to using a single type of urban morphology? (2) What is exactly the day–night contrast regarding the relative importance of 2D and 3D urban morphology in regulating local thermal environment? (3) How does the relative importance of 2D and 3D structures of building and tree vary with spatial scale?

Considering these knowledge gaps, this study aims to investigate systematically both the separate and combined effects of 2D and 3D urban morphology (including both building and tree) at various spatial scales. The day–night contrast of such effects will also be one of our emphasis. The remainder of this paper is organized as follows. The study area and data source are shown in Section 2. Section 3 describes the methods, including the illustration of the indicators for 2D and 3D urban morphology, and the statistical analysis. The separate and combined impacts of building and tree on the thermal environment as well as their scale sensitivity are presented and discussed in Sections 4 and 5, respectively. Section 6 summarizes the conclusions. This study may provide valuable insights for urban planners in designing heat mitigation strategies over urban surfaces.

2. Study area and data

2.1. Study area

As the capital of Jiangsu Province, China, Nanjing city is situated in the center of the lower reaches of the Yangtze River and has a population of more than 8.2 million. Nanjing is characterized by a subtropical monsoon climate with four pronounced seasons, and is acknowledged as one of the “Four Furnace Cities" in China due to its hot and humid summer [36]. The monthly mean temperature ranges from 2.2 °C in January to 28.6 °C in July, with a maximum temperature more than 40 °C. It is reported that an increasing number of hot days and nights were observed, and heat waves are predicted to be more frequent in Nanjing [37]. Therefore, research into the impacts of building and tree on the urban thermal environment of Nanjing was considered as an ideal case. The study area in this research is located in the central downtown of Nanjing, covering a total of area about 205 km^2 (Fig. 1).

2.2. Data and pre-processing

2.2.1. Land surface temperature

Given that our study was devoted to explore how building and tree interact to impact diurnal LST, ASTER LST was used owing to its ability of providing daytime and nighttime LSTs with high spatial resolution. In this work, LST data was obtained from ASTER surface kinetic temperature product[1] (i.e., AST 08) with the unit of 90 m (https://lpdaac.usgs.gov/products/ast_08v003/). The ASTER surface kinetic temperature is retrieved by adopting Planck’s Law using the emissivity values from temperature-emissivity separation (TES) approach, which utilizes atmospherically correct ASTER surface radiance (TIR) data. The absolute accuracy of ASTER LST was within ±1.5 K [12,14,38]. To make the acquisition time of LST data as closest as possible to the date of airborne LiDAR data, together with the data quality and availability, daytime LST image was obtained about five hours and forty one minutes after sunrise with 11:00 a.m on May 1, 2011, while nighttime LST image was acquired about five hours and six minutes after sunset with 22:19 p.m on April 4, 2011. The surface kinetic temperature was converted into Celsius degree for further LST analysis (Fig. 2(c) and (d)). Although there was an approximate two-year time difference between the acquisition of IKONOS-2 and LST images, limited change in the spatial pattern of building and tree can be observed between 2009 and 2011, owing to that our study area was confined in relatively stable downtown of Nanjing.

2.2.2. LiDAR data and IKONOS-2 image

The data used in this work, as shown in Table 1, was collected from four different sources. Airborne LiDAR data was employed to improve classification performance and obtain the vertical structures of urban morphology. The acquisition time of LiDAR data was on April 21 and 22, 2009, and the mean density of LiDAR data was approximately 4 points/m^2. We employed 2D grids with 3 m and 3.2 m spatial resolution to process LiDAR data. The digital elevation model (DEM) was produced by applying a triangular irregular network to ground points, while by summarizing elevation of the points of the first return, we obtained the digital surface model (DSM). A normalized DSM (nDSM) layer, representing only the above-ground feature, was produced by subtracting the DSM with DEM. LiDAR-derived products

[1] ASTERTIRPointingAngle and ASTERSceneOrientationAngle were 8.57° and 9.67° for daytime LST (11:00 a.m) and −8.56° and 170.33° for nighttime LST (10:19 p.m). ASTERTIRPointingAngle represents the pointing angle of the ASTER Thermal Infrared (TIR) sensor, while ASTERSceneOrientationAngle denotes the azimuth angle made by the meridian at the ASTER scene center and the along-track direction, rotating from North toward East.

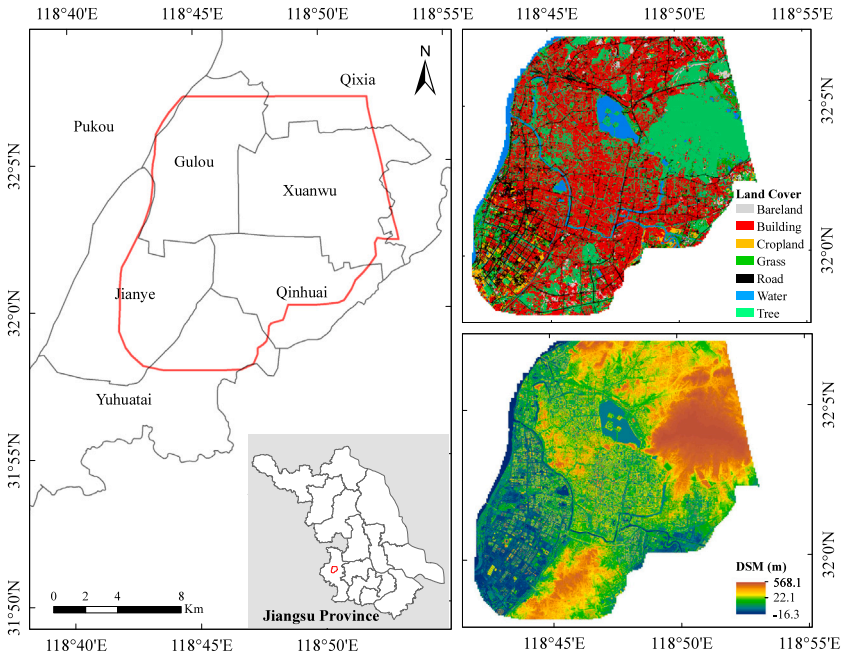

Fig. 1. (a) Location of the study area; (b) Land cover map of the study area, achieved by the combination of IKONOS-2 and LiDAR data; (c) normalized digital surface model (nDSM) derived from LiDAR data.

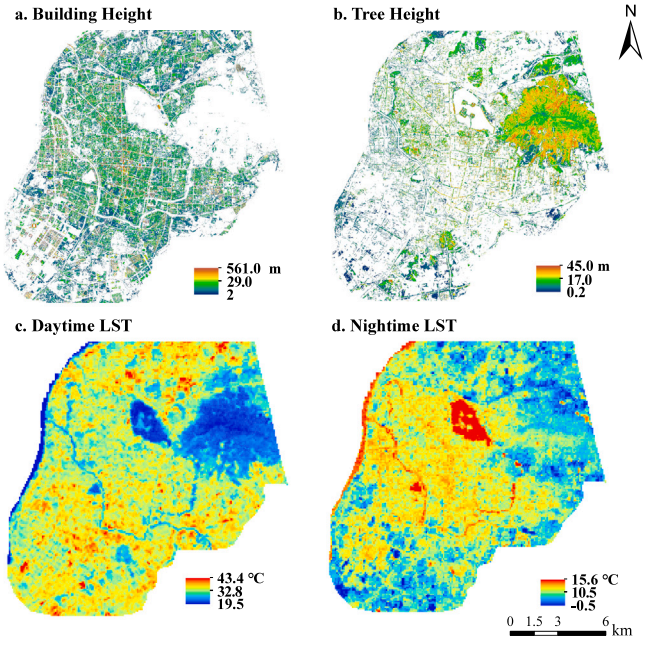

Fig. 2. (a) Building height; (b) Tree height; (c) and (d) are daytime ASTER land surface temperature (May 1, 2011) and nighttime ASTER land surface temperature (April 4, 2011), respectively.

with a pixel size of 3.2 m were used to integrate with the IKONOS-2 image to derive land cover map, whereas 3 m LiDAR-derived products were produced to measure the 3D information of building and tree (Fig. 2(a) and (b)).

IKONOS-2 multispectral satellite imagery used was acquired on June 18, 2009. The image consists of four multispectral channels with a spatial resolution of 3.2 m covering blue (445–516 nm), green (506–595 nm), red (632–698 nm) and near-infrared (757–853 nm). IKONOS-2 image enabled us to map high-resolution urban land cover. Note that all the data mentioned above were co-georeferenced to enable the consistency of the corresponding spatial position.

2.2.3. Land cover map

Urban land cover map was achieved by combining IKONOS-2 and LiDAR data (Fig. 3), since the data fusion can compensate for the limitations of each other to improve classification accuracy. In this work, we proposed to use an object-based approach to classify urban land cover. First, image objects were created with multiresolution segmentation, which is based on four spectral bands and LiDAR-derived DEM, DSM, nDSM and intensity layers. Second, a wide variety of object features were calculated, such as LiDAR-derived intensity and return features. Finally, the object-based land cover classification was implemented using Random Forest classifier. Two parameters should be carefully determined for Random Forest: the number of trees (n_{tree}) and the number of features employed for the best split at each mode (m_{try}). n_{tree} and m_{try} were set to 500 and the square root of the number of input features, respectively. More detailed information about parameter setting can be accessed in [39]. The classified urban land cover with 3.2 m spatial resolution was documented in Fig. 1(b). The overall accuracy of urban land cover was achieved by 99.35%, and class-specific accuracies ranged from 98.85% to 99.92%. The producer's and user's accuracies were 99.35% and 99.0% for building and 98.85% and 99.13% for tree. The more detailed information, which is related to ground reference and classification accuracy, can be referenced in Supplementary Table A.1 and A.2. For further analysis, the land cover map was resampled to the spatial resolution of 3 m.

3. Methodology

3.1. Measuring the 2D landscape pattern of building and tree

Previous research suggested that the landscape pattern (i.e., composition and configuration) had significant impacts on UHI [19,40,41]. Composition delineates the features related to the abundance and diversity of patches, while configuration refers to the spatial arrangement of patches. Based on the principles of interpretable, minimum redundancy, theoretical and practical significance [26,42], six widely-used landscape metrics were selected to measure 2D landscape pattern of building and tree and were mathematically displayed in Table 2, including one composition metrics: percentage of landscape (PLAND), and five configuration metrics: largest patch index (LPI), edge density

Table 1
Data used in this research (Data description).

Satellite data	Date	Resolution	Analysis
IKONOS-2	6/18/2009	3.2 m	Land cover classification
Airborne LiDAR	4/21/2009 4/22/2009	4.10 points/m^2 4.23 points/m^2	Land cover classification and 3D urban morphology
Google Earth	2009	/	Ground reference for land cover mapping
ASTER(AST_08)	04/04/2011 14:19:28Z	90 m	Land surface temperature
	05/01/2011 03:00:46Z	90 m	

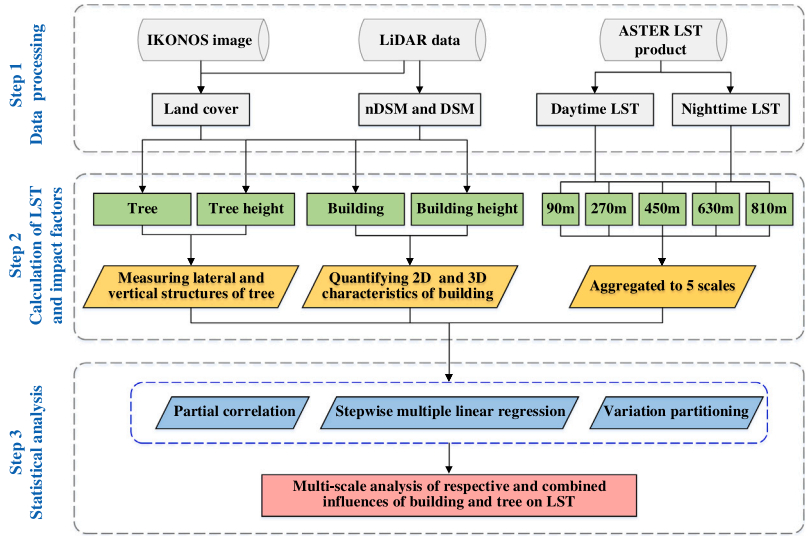

Fig. 3. Conceptual flowchart of the data analysis.

(ED), patch density (PD), patch cohesion index (COHESION) and mean patch shape index (SHAPE_MN). The software Fragstats 4.2 was used to calculate the landscape metric mentioned above, using the 8-cell neighborhood rule (http://www.umass.edu/). Moreover, edge density was calculated under the condition that no boundary interface was counted as edge.

3.2. Indicators of 3D urban morphology

In this study, numerous indicators were selected to quantify 3D morphology. Table 3 summarized the 3D characteristic indicators of building and tree adopted in this study. All these indices were computed based on the land cover map, DSM and nDSM mentioned above (see Section 2.2.2). BH_Mean and TH_Mean indicated respectively the mean building and tree height above ground. SVF_b was considered as the potential factors. SVF suggests the ratio of the radiation received by a planar surface to that emitted from the entire hemispheric environment [44]. Therefore, when exploring the separate impact of building on LST, partial SVF (i.e., SVF_b), which describes the obstructions of sky raised by building, was explored in this work to remove action of tree. It was calculated using the Urban Multi-scale Environmental Predictor model, which can be used for various applications in the light of climate change mitigation [45]. Furthermore, even though SVF_t, which represents of the block of sky raised by tree, is an potential impact factor of LST, it was not computed in this work, owing to the lack of accurate transmissivity of light through vegetation and percent of tree canopy height.

3.3. Statistical analysis

Given the pixel size of LST data and the spatial scales used in the previous studies [26,46], the entire landscape of the study area was divided into five sizes of statistical units: 90 m×90 m (i.e., the equal pixel size of ASTER LST), 270 m×270 m, 450 m×450 m, 630 m×630 m and 810 m×810 m, and the mean LST along with influencing factors were computed for each statistical unit (Fig. 3). To analyze the influences of 2D and 3D urban morphology on diurnal LST, a series of statistical approaches were conducted. Partial correlation was first performed to evaluate the relation between diurnal LST and building or tree, as it can avoid the covariate impacts between 2D and 3D explanatory metrics [34,47]. Related results and discussions were presented in the supplementary file (Supplementary Section A.2 and A.3).

Next, stepwise multiple linear regression model was used to explore how building and tree exerted on diurnal LST separately and combinedly, which were performed with the "MASS" package of R. Independent variables entered the final regression models were selected by Akaike information criterion (AIC) and stepwise selection, which is a combination of the forward and backward selection techniques. Adjusted R^2 was selected to estimate the explanatory power of models, while standardized coefficients were employed to measure the relative contribution of each variable to diurnal LST. To investigate the separate impacts of building and tree on LST, we built three regression models for building and tree, respectively: Model-1 with 2D building/tree structure; model-2 with 3D building/tree structure; and model-3 with 2D and 3D building/tree structures. On the other hand, four regression models were built to clarify how building and tree interacted to impact the diurnal LST, which can be formulated as a function of: 2D building and tree structures; 2D building and tree structures together with 3D building structure; 2D building and tree structures combined with 3D tree structure, and 2D and 3D building and tree structures. Moreover, to validate the performances of these models, 70% of data were randomly selected as training set, and the remaining 30% data were employed for validation. Root mean square error (RMSE) was used as an accuracy metric to evaluate these estimations [48]. We repeated 100 times to report the average value of RMSE to avoid biased estimation.

Table 2
Landscape metrics used in this study to quantify landscape pattern of urban building and tree [43].

Metrics (abbreviation)	Definition	Calculation (unit)	Variable name
Percentage of landscape (PLAND)	Percent cover of a given land cover class within an analysis grid	$PLAND_i = \frac{\sum_{j=1}^{n} a_j}{A} \times 100$ (%)	PER_Build, PER_Tree
Patch density (PD)	Density of landscape patches within an analysis grid.	$PD_i = \frac{n}{A} \times 10,000 \times 100$ (n/km^2)	PD_Build, PD_Tree
Largest patch index (LPI)	The area proportion of the largest building/tree patch within an analysis grid.	$LPI = \frac{max a_j}{A} \times 100$	LPI_Build, LPI_Tree
Edge density (ED)	Sum of patch perimeters per hectare within an analysis grid.	$ED_i = \frac{\sum_{j=1}^{n} e_j}{A} \times 10,000$ (m/ha)	ED_Build, ED_Tree
Mean patch shape index (SHAPE_MN)	The average value of shape index of landscape patches within an analysis grid.	$SHAPE\_MN_i = \frac{1}{n} \sum_{j=1}^{n} \frac{p_j}{4 \times \sqrt{a_j}}$	SHAPE_MN_Build, SHAPE_MN_Tree
Patch cohesion index (COHESION)	A measure of physical connectedness for landscape patches within an analysis grid.	$COHESION_i = \left[1 - \frac{\sum_{j=1}^{n} p_j^*}{\sum_{j=1}^{n} p_j^* \sqrt{a_j^*}}\right] \times \left[1 - \frac{1}{\sqrt{Z}}\right] \times 100$	COHESION_Build, COHESION_Tree

A = the area of an analysis grid; n = number of landscape patches within an analysis grid; e_j = lengths of edge segments of landscape patch j; P_j = perimeter of landscape patch j; a_j = area of landscape patch j; P_j^* = perimeter of landscape patch j regarding to number of cell surfaces; a_j^* = area of landscape patch j with respect to number of cells; Z = total number of cells within an analysis grid.

Table 3
Summary of the 3D building and tree characteristic metrics considered in this research.

Categories	Metrics (abbreviation)	Description	Equations
Building	Mean building height (BH_Mean)	Mean building height within a statistical unit.	$BH\_Mean_i = \frac{\sum_{j=1}^{n} BH_j}{n}$
	Maximum height of buildings (BH_Max)	Maximum height of building within a statistical unit.	$BH\_Max_i = Max(BH_j), j = 1, 2, 3, \ldots, n$
	Variance of building height (BH_SD)	Standard deviation of building height within a statistical unit.	$BH\_SD_i = \sqrt{\frac{\sum_{j=1}^{n} (BH_j - BH\_mean_i)^2}{n}}$
	Normalized variance of building height (NBH_SD)	The ratio of variance to mean of building height within a statistical unit.	$NBH\_SD_i = \frac{BH\_SD_i}{BH\_Mean_i}$
	Sky view factor achieved by buildings (SVF_b)	Sky view factor responsible for blocking of sky by buildings.	$SVF\_Build_i = \frac{\sum_{j=1}^{n} SVF\_Build_j}{n}$
	Building height value at 10th percentile (BH_P10)	The 10th percentile value of building height, which is derived from DSM.	$BH\_P10_i = 10thPercentile(BH\_DSM_j)$
	Building height value at 90th percentile (BH_P90)	The 90th percentile value of building height, which is derived from DSM.	$BH\_P90_i = 90thPercentile(BH\_DSM_j)$
Tree	Mean tree height (TH_Mean)	Mean of tree canopy height within an analysis grid	$TH\_Mean_i = \frac{\sum_{j=1}^{n} TH_j}{n}$
	Maximum height of tree canopy (TH_Max)	Maximum of tree canopy height within an analysis grid.	$TH\_Max_i = Max(TH_j), j = 1, 2, 3, \ldots, n$
	Variance of tree canopy height (TH_SD)	Standard deviation of tree canopy height within an analysis grid.	$TH\_SD_i = \sqrt{\frac{\sum_{j=1}^{n} (TH_j - TH\_mean_i)^2}{n}}$
	Normalized tree canopy height variance (NTH_SD)	The ratio between variance and mean in terms of tree canopy height within an analysis grid	$NTH\_SD_i = \frac{TH\_SD_i}{TH\_Mean_i}$
	10th percentile tree height value (TH_P10)	The 10th percentile value of DSM-derived tree height.	$TH\_P10_i = 10thPercentile(BH\_DSM_j)$
	90th percentile tree height value (TH_P90)	The 90th percentile value of DSM-derived tree height.	$TH\_P90_i = 90thPercentile(BH\_DSM_j)$

BH_j = building height calculated for grid j within the statistical unit i; SVF_Build_j = sky view factor calculated based on building for grid j within the analysis grid i; BH_DSM_j represents the DSM-derived building height. TH_j = tree canopy height computed for grid j within the statistical unit i; SVF_Tree_j = sky view factor calculated based on tree for grid j within the analysis grid i; TH_DSM_j corresponds to the height of DSM-derived tree height.

Finally, to distinguish the relative importance of different sets of predictor variables while exploring the impacts of building and tree on LST, variation partition was used. Variation partition could divide LST variation into three major fractions [49,50]: (1) unique effects of each independent variable; (2) common effects of in all possible combinations of independent variables; (3) the unexplained variation in LST. Common effects arise because there was correlation between explanatory variables, and thus their impacts on the LST cannot be statistically split [49].

4. Results and analysis

4.1. Spatial characteristics of diurnal LST and its drivers

Large discrepancies existed for the spatial patterns of daytime and nighttime LSTs (Fig. 2(c) and (d)). During the day, areas with high LST were concentrated mainly in the southern and northern regions, whereas at night, they were mostly located in the central part. The daytime LST ranged from 19.45 °C to 43.35 °C, with a mean of 31.08 °C and standard deviation of 2.31 °C. During the night, the average and standard deviation of LST were respectively 9.01 and 1.66 °C (Supplementary Table A.3, A.4, A.5 and A.6). The analytical unit of 90 m×90 m was taken as case-study to elucidate the spatial pattern of building and tree. Building and tree covered 43.97% and 30.12% of the study area, respectively. The mean building height varied from 2.0 m to 130.33 m, while the mean and SD values of tree height were 8.70 m and 4.86 m separately. The patch and edge density of building were higher than that of tree, suggesting that building patches were relatively more fragmented (Supplementary Fig. A.1).

4.2. Effects of 2D and 3D characteristics of building on LST

The separate and combined impacts of 2D and 3D building morphology on diurnal LST were firstly investigated, as is shown in Fig. 4. Despite of day and night, the explanatory power of regression models became stronger at a larger statistical unit. This may be due to that, at high resolution, some units may be clearly hit by the sun while some other are in the shade. Then larger is the unit, more chance you have to eliminate the shading variability due to the spatial variation of urban fabric. In contrast, with the increase of statistical size, differences of thermal characteristics between analytical units become smaller, leading to more nighttime LST variation be explained by building.

During the day, the model, using both 2D and 3D building metrics, obtained the highest R^2. The regression model with only the 3D building metrics explained the lowest variation in daytime LST across different scales. At night, the regression model with only 3D building

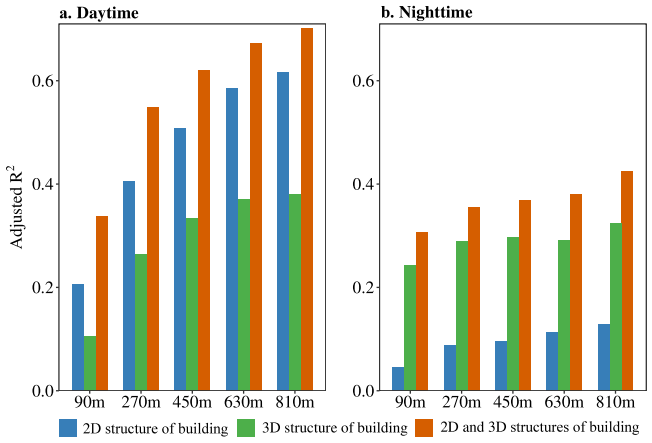

Fig. 4. Adjusted determinant coefficients (R^2) of stepwise multiple linear regressions of 2D and 3D building characteristics with daytime and nighttime LSTs.

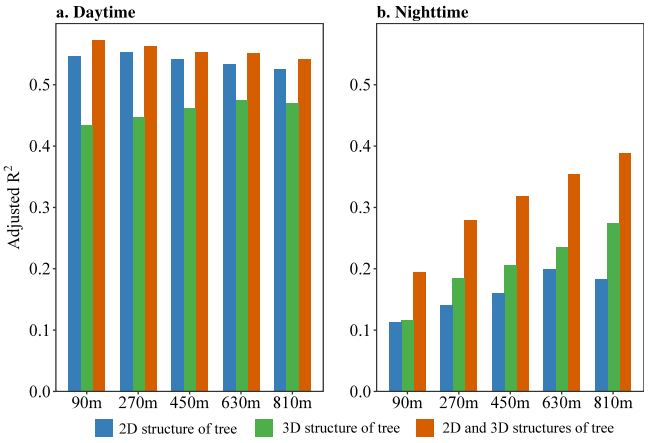

Fig. 5. Adjusted R^2 of stepwise multiple linear regressions of horizontal and vertical structure of tree with daytime and nighttime LSTs.

metrics accounted for more variation, compared to the model with only 2D building metrics (Fig. 4(b)). 2D and 3D building metrics considered together can explain the highest fraction of variation in nighttime LST. Moreover, the regression model with 2D and 3D building structures achieved lower RMSE for both day and night, compared to the models with only 2D or 3D building structure (Table 4). Next, the results, which is related to the unique contributions of 2D and 3D building metrics to explaining the LST variation, indicated that 2D building metrics alone explained the largest fraction of the LST variation in the daytime, whereas the contribution of the unique effect of 3D building metrics to nighttime LST was the most important (Supplementary Fig. A.2).

4.3. Impacts of horizontal and vertical structures of tree on LST

Results of regression models indicated that much more variation in daytime LST can be explained by tree than in nighttime LST (Fig. 5). During the day, the adjusted R^2 demonstrated the impacts of horizontal tree variables on LST were stronger than that of vertical tree variables. The model, including horizontal and vertical tree variables, accounted for a larger proportion of LST variation at night, but an inverse trend was demonstrated during the day. The model with 2D and 3D tree structures tended to explain less variation in daytime LST. This is because the cooling effect of tree canopy within larger statistical units is weakened by the impact of surrounding landscape [51]. In contrast, at night, LST was mainly dominated by vertical tree structure. An increase in analytical unit tend to compromise the differences of vertical tree structure between analytical units, resulting in more LST to be accounted for. However, there are some differences in the scale-dependent response of tree to daytime and nighttime LSTs. During the day, the explanatory power of the regression model with vertical tree variables increased modestly as statistical size increased, but opposite trends were observed from the other two models (Fig. 5(a)). In contrast to daytime LST, the larger the statistical size, the more variation in nighttime LST tree could explain for all three models (Fig. 5(b)). In addition, RMSE suggested that regression model with 2D and 3D tree structures performed better in estimating daytime and nighttime LSTs (Table 4).

Results of variation partitioning implied that the unique effect of horizontal tree structure played a more important role than that of vertical tree structure in influencing daytime LST (Supplementary Fig. A.4). In contrast, vertical tree structure alone explained more nighttime LST variation than horizontal tree structure across all statistical scales. Another one was that there was a large difference between daytime and nighttime LSTs, in terms of explanatory power common to both horizontal and vertical variables, which results from the correlation between horizontal and vertical tree variables as shown in Supplementary Fig. A.3.

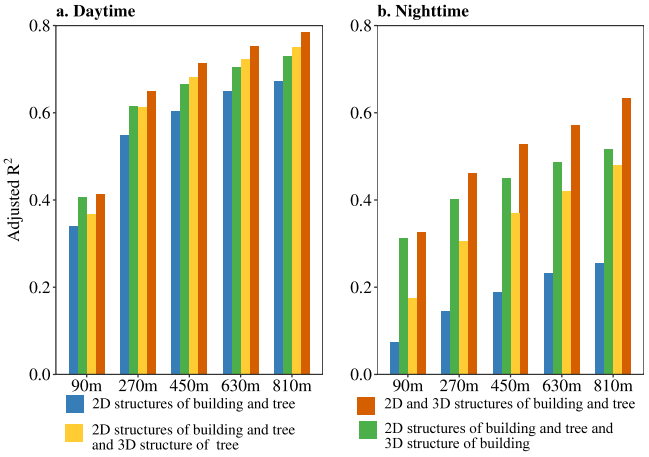

Fig. 6. Adjusted R^2 of stepwise multiple linear regressions with daytime and nighttime LSTs, while jointly considering building and tree.

4.4. Insight into the coupling influences of building and tree on LST

It can be observed from Fig. 6, combining 2D and 3D metrics of building and tree obtained the best R^2, and the least LST variation was explained by the model with only 2D metrics of building and tree, regardless of daytime and nighttime. The adjusted R^2 of the four models increased as the statistical size increased. During the day, when the statistical size was larger than 90 m, the LST variation was better explained by the models with the combination of all 2D metrics and 3D tree metrics, compared to the model with the combination of all 2D metrics and 3D building metrics. However, at night, the explanatory power of the model with only all 2D metric can be enhanced better by adding 3D building metrics than by adding 3D tree metrics at all statistical scales. The model with all 2D metrics achieved an RMSE of 1.32 for nighttime LST, and RMSE was decreased to 0.94 by adding all 3D metrics at 810 m (Table 5).

Then, two different mechanisms were utilized to quantify the relative contributions of 2D and 3D structures to explaining LST variation. One way was to divide explanatory variables into two groups: 2D building and tree metrics, and 3D building and tree metrics. During the day, 2D structures of building and tree alone explained larger proportion of LST variation across all statistical scales, compared to their 3D structures (Supplementary Fig. A.5). Furthermore, there was a large proportion of variation in daytime LST, which was accounted for by the common impacts of 2D and 3D structures. In contrast, variation

Table 4
RMSE values of regression models based on 2D and 3D structures of building or tree.

Time	Scale	Building			Tree		
		2D Structure	3D Structure	2D + 3D structures	2D Structure	3D Structure	2D + 3D structures
Daytime	90 m	2.06	2.19	1.88	1.96	2.19	1.91
	270 m	1.88	2.09	1.65	1.85	2.06	1.83
	450 m	1.78	2.06	1.56	1.85	1.99	1.81
	630 m	1.65	2.06	1.51	1.83	1.91	1.81
	810 m	1.62	2.07	1.50	1.81	1.91	1.80
Nighttime	90 m	1.62	1.44	1.38	1.61	1.61	1.53
	270 m	1.47	1.30	1.24	1.45	1.41	1.33
	450 m	1.42	1.26	1.19	1.40	1.36	1.26
	630 m	1.39	1.23	1.19	1.32	1.28	1.19
	810 m	1.37	1.24	1.19	1.31	1.29	1.17

in nighttime LST was mainly accounted for by the unique impact of 3D building and tree structures.

Another way was to divide explanatory variables into four sets: 2D building metrics, 3D building metrics, horizontal tree metrics, and vertical tree metrics. As can be seen from Fig. 7, variation in daytime LST was best explained by the unique effect of 2D building metrics at all statistical scales, regarding the unique fractions. In addition, the independent contribution of 2D building metrics was larger than that of 3D building metrics. Vertical tree variables independently captured more variation in daytime LST compared to horizontal tree variables at all scales except the statistical size of 90 m.

The result of the variation partition at night was presented in Fig. 8. As for the unique effects, 3D building metrics alone accounted for the highest amount of variation in nighttime LST. The nighttime LST variation uniquely explained by 3D building metrics was larger than that of 2D building metrics across all five statistical scales, which is contrary to the finding during the day. With regard to tree, much more nighttime LST variation can be explained by horizontal tree variables alone than by vertical tree variables, when the statistical size was smaller than 810 m. Moreover, the unique effect of the vertical tree variable was stronger with the increase of statistical size.

5. Discussion

5.1. The extent to which combining 2D and 3D structures improve the explanatory power of LST variation compared to individual structures

With respect to the separate and interacting impacts of building and tree on LST, the differences in explaining LST variation remain poorly understood when 2D and 3D structures were jointly and separately considered. In this study, compared to 2D and 3D structures used separately, the combination of two groups of variables could explain more in LST variation, which is similar to some previous research [31,34,52]. However, different degrees of the enhancement were observed for day and night. As for the separate impact of building on daytime LST across five statistical scales (Fig. 4), combining 2D and 3D building structures improved the explanatory powers of LST by 8.5%–14.5% and 23.2%–32.1%, respectively, compared to using separate 2D and 3D structures. When horizontal and vertical structures of tree were put together to explain LST variation (Fig. 5), the explanatory ability of horizontal or vertical structure in LST was enhanced more pronounced at night than during the day. The model with vertical structure of tree increased the explanatory power of nighttime LST by 7.1%–13.8% with the inclusion of horizontal tree structure. By adding vertical tree structure to the model with horizontal tree structure, 8.1%–20.5% more nighttime LST variation was captured.

When compared to the combined impact of building and tree on LST (Fig. 6), the explanatory powers of the model with 2D structures of building and tree were improved by 7.3%–11.1% and 25.3%–37.7% for daytime and nighttime LSTs separately. Another important finding was that the combination of building and tree explained a larger proportion of LST variation both in the day and night at all statistical sizes, except 90 m, compared to their separate impacts. This indicated it needs to explore the combined impacts of building and tree on LST with finer resolution LST data [53]. The maximum joint explanatory power of building and tree reached at the largest statistical size (810 m), but a portion of daytime LST variation (21.5%) and nighttime LST variation (36.7%) remained unexplained. This suggested the existence of a more complex mechanism underlying the spatial pattern of diurnal LST, and that more influencing factors such as water bodies and building material need to be considered [34,54,55].

5.2. The separate impacts of building and tree on LST: diurnal contrast and scale-dependence of relative importance of 2D and 3D structures

As for the impact of building on daytime LST, 2D building metrics showed a stronger influence on daytime LST compared to 3D building metrics, which is consistent with the study conducted in Wuhan, China [34]. It indicated that, during the day, though 3D building structure could impact the amount of incoming solar radiation and heat dissipation, it was constrained by landscape pattern of building [32]. However, some previous studies found the contradictory trend [33], owing to the difference in the climatic zones [56]. In contrast, 3D building metrics acted as a more important role than 2D building metrics in impacting nighttime LST. When the separate impact of tree on daytime LST was investigated, horizontal tree variables affected LST more than vertical tree variables. However, opposite trend was found at night.

Regression models with 2D and 3D building metrics showed that PER_Build was the most important factor for predicting daytime LST across all scales (Supplementary Table A.7). Moreover, the relative importance of PER_Build in predicting daytime LST increased with increasing statistical size, which is consistent with some previous study [32]. PER_Build had a strong positive correlation with daytime LST across all statistical scales because higher PER_Build could increase sensible flux but reduce latent flux [57]. However, the scale-dependence variation in the major predictor of nighttime LST was notable, where the most important factors were SVF_b at the statistical size less than or equal to 450 m, and were BH_Mean and BH_SD respectively for 630 m and 810 m. BH_Mean had positive relationships with nighttime LST across all statistical scales (Supplementary Table A.7), which is consistent with the conclusions of other studies [58–60]. BH_SD had a significantly negative impact on nighttime LST, owing to that higher BH_SD may benefit the increase of wind circulation to release heat [27,61]. SVF_b was negatively correlated with nighttime LST, which was determined by the combined impacts of the following two processes. Higher SVF_b always corresponded to the more incoming solar radiation to reach the surface, and thus increased the LST [34]. In contrast, higher SVF_b could decrease LST by improving air circulation and the loss of longwave radiation [29].

The relationships between tree and LST determined that PER_Tree was the most important determinant of daytime LST for the statistical size of 90 m and 270 m (Supplementary Table A.8), which is consistent with many previous studies [18,26,62]. When the statistical size was larger than 270 m, daytime LST was primarily influenced by LPI_Tree.

Table 5
RMSE values of regression models based on 2D and 3D structures of building and tree.

Time	Scale	2D Building + 2D Tree structures	2D Building + 2D Tree + 3D Building structures	2D Building + 2D Tree + 3D Tree structures	2D Building + 3D Building + 2D Tree + 3D Tree structures
Daytime	90 m	1.82	1.73	1.78	1.71
	270 m	1.64	1.52	1.53	1.45
	450 m	1.58	1.46	1.42	1.35
	630 m	1.52	1.44	1.39	1.34
	810 m	1.53	1.48	1.39	1.31
Nighttime	90 m	1.58	1.36	1.50	1.35
	270 m	1.43	1.20	1.30	1.14
	450 m	1.36	1.11	1.20	1.04
	630 m	1.28	1.08	1.15	1.00
	810 m	1.32	1.09	1.12	0.94

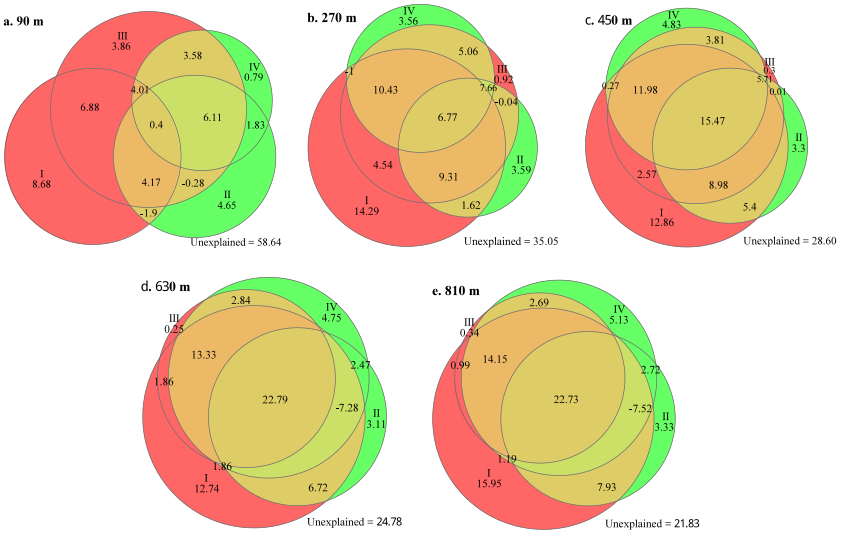

Fig. 7. The unique and common impacts of 2D and 3D characteristics of building and tree on daytime LST. (I refers to 2D characteristics of building; II refers to 3D characteristics of building; III denotes horizontal structures of tree; IV denotes vertical structures of tree.).

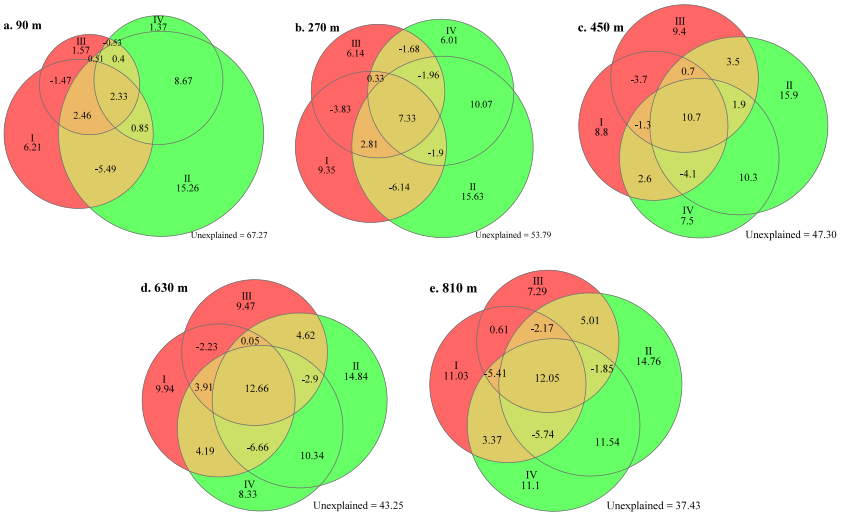

Fig. 8. The unique and common impacts of 2D and 3D characteristics of building and tree on nighttime LST. (I refers to 2D characteristics of building; II refers to 3D characteristics of building; III denotes horizontal structures of tree; IV denotes vertical structures of tree.).

However, nighttime LST was primarily influenced by PER_Tree across when the size of statistical scale was larger than 270 m. Nevertheless, this study found that the tree cooling efficiency, which is defined as the increase in LST with the increase of 1% tree cover [26,63], was higher during the day than at night at the finest scale (90 m), but an opposite trend was shown at other statistical scales.

5.3. Sensitivity of relative importance of 2D and 3D structures to scale and diurnal LST regarding the combined impact of building and tree

Our findings indicated that 2D structures of building and tree played a more important role in shaping daytime LST compared to these 3D structures, but the opposite trend was presented at night (Supplementary Fig. A.5). More specially, 2D and 3D building indicators showed

the strongest impact on daytime and nighttime LSTs, respectively. Horizontal tree variables affected nighttime LST more than vertical tree variables with the statistical scale ranging from 90 m to 630 m. However, vertical tree structure played a more important role in predicting daytime LST than that of horizontal tree structure, when the statistical scale exceeded 90 m. Moreover, this study indicated the unique effect of 2D building metrics was stronger than that of 3D building metrics at the scales, ranging from 270 m to 810 m, for day–night LST difference. However, vertical tree metrics alone accounted for more variation in day–night LST difference than horizontal tree variables across all scales (Supplementary Fig. A.6, A.7 and A.8).

By exploring the relative importance of the individual influencing factor, the results suggested that, daytime LST was mainly governed by PER_Build for all statistical sizes (Supplementary Table A.9). The most important determinant of nighttime LST was influenced by statistical size. SVF_b appeared as the most determinative variable of nighttime LST at the statistical size less than or equal to 270 m, whereas PER_Tree played the most vital role at the statistical sizes from 450 m to 810 m.

5.4. Limitations

This research has showed the necessity of exploring the UHI effect with multi-dimensional and multiscale. However, further studies need to be carried out to fully understand how building and tree affect diurnal LST in the three-dimensional space. First, while maintaining the same weather conditions used in this study, we would like to use multiple daytime and nighttime thermal images to investigate whether our results would hold true. Second, considering the impact of SVF_t on LST, further research should be conducted to calculate precise SVF_t and explore how it impacts the diurnal LST [29]. Third, previous research has demonstrated that the cooling impact varied largely between different tree species [28]. Further studies should take tree species into account in the effect of urban tree on LST. Finally, given that the UHI effect varied across different geographic regions (e.g., climatic zones and arid–humid areas), similar research should be conducted to compare with our conclusions [56].

6. Conclusions

Since urban environments are complex multi-dimensional settings, the impacts of urban land cover on UHI should incorporate not only 2D characteristics, but also 3D structure. Comprehensive analyses, which aimed at distinguishing the separate and combined effects of building and tree on diurnal LST associated with their scale-dependence in the multi-dimensional urban environment, are certainly beneficial to ameliorate the UHI effect. This research revealed that, despite of the separate and combined effects of building and tree, the combination of 2D and 3D characteristics could better predict LST than features of a single dimension for both day and night. As for the combined impacts of building and tree across different spatial scales, combining 2D and 3D structures improved the explained LST variation by 7.3%–11.1% and 25.3%–37.7% for day and night respectively, when compared to using their 2D structures only. Regarding the separate impact of building, 2D indicators affected more daytime LST than 3D indicators, but an inverse trend was demonstrated for nighttime LST. PER_Build affected most daytime LST at all spatial scale, but the most important indicators of nighttime LST was more scale-dependent. With respect to the separate impact of tree, during the day, 2D structure of tree played a more important role in predicting LST compared to its 3D structure, and the relative contribution of 3D structure of tree was very limited. At night, 3D tree structure explained a larger proportion of LST variation compared to 2D tree structure. When building and tree were considered together to predict LST, daytime and nighttime LSTs were primarily governed by 2D and 3D structure of building, respectively. The most important determinant of daytime LST is PER_Build across all statistical scales. Contrary to daytime LST, the most important factor of nighttime LST was influenced by changing statistical sizes, including SVF_b, PER_Tree. Scale-dependence variation, which is related to the most important indicator of tree structure, was notable for both daytime and nighttime LSTs. Furthermore, this research demonstrated that separate and combined effects of building and tree on LST, except the separate impact of tree on daytime LST, became stronger as the statistical scale increased. Consequently, our study provided some novel insights into the assessment of the impacts of urban land cover on UHI to enhance the resilience of the urban environment to future climate change. It is necessary to take 3D structure of land cover into the effect of urbanization on UHI, and the choice of scale, which land cover and LST interacts, was closely related to the mitigation of UHI effect.

Declaration of competing interest

The authors declare that they have no known competing financial interests or personal relationships that could have appeared to influence the work reported in this paper.

Acknowledgments

This work was supported by the Strategic Priority Research Program Project of the Chinese Academy of Sciences (Grant No. XDA23040100), China Postdoctoral Science Foundation (No. 2019M661885), Jiangsu Province Distinguished Professor Project (Grant No. R2018T20), Startup Foundation for Introducing Talent of NUIST, China (Grant No. 2243141801036), the program B for outstanding PhD candidate of Nanjing University, China (No. 201701B019), and Natural Science Foundation of China (No. 41571350).

Appendix A. Supplementary data

Supplementary material related to this article can be found online at https://doi.org/10.1016/j.buildenv.2021.107650.

References

[1] T.R. Oke, The energetic basis of the urban heat island, Q. J. R. Meteorol. Soc. 108 (455) (1982) 1–24.
[2] L. Zhao, X. Lee, R.B. Smith, K. Oleson, Strong contributions of local background climate to urban heat islands, Nature 511 (7508) (2014) 216.
[3] T.R. Oke, City size and the urban heat island, Atmos. Environ. (1967) 7 (8) (1973) 769–779.
[4] H. Akbari, M. Pomerantz, H. Taha, Cool surfaces and shade trees to reduce energy use and improve air quality in urban areas, Sol. Energy 70 (3) (2001) 295–310.
[5] D.A. Graham, J.K. Vanos, N.A. Kenny, R.D. Brown, The relationship between neighbourhood tree canopy cover and heat-related ambulance calls during extreme heat events in Toronto, Canada, Urban For. Urban Green. 20 (2016) 180–186.
[6] C. Mora, B. Dousset, I.R. Caldwell, F.E. Powell, R.C. Geronimo, C.R. Bielecki, C.W. Counsell, B.S. Dietrich, E.T. Johnston, L.V. Louis, et al., Global risk of deadly heat, Nature Clim. Change 7 (7) (2017) 501–506.
[7] P.K. Rao, Remote sensing of urban "heat islands" from an environmental satellite, Bull. Am. Meteorol. Soc. 53 (7) (1972) 647–648.
[8] M.L. Imhoff, P. Zhang, R.E. Wolfe, L. Bounoua, Remote sensing of the urban heat island effect across biomes in the continental USA, Remote Sens. Environ. 114 (3) (2010) 504–513.
[9] Q. Weng, Thermal infrared remote sensing for urban climate and environmental studies: Methods, applications, and trends, ISPRS J. Photogramm. Remote Sens. 64 (4) (2009) 335–344.
[10] R. Hamdi, G. Schayes, Sensitivity study of the urban heat island intensity to urban characteristics, Int. J. Climatol. 28 (7) (2008) 973–982.
[11] H. Ding, A.J. Elmore, Spatio-temporal patterns in water surface temperature from Landsat time series data in the Chesapeake Bay, USA, Remote Sens. Environ. 168 (2015) 335–348.
[12] M. Abrams, The advanced spaceborne thermal emission and reflection radiometer (ASTER): data products for the high spatial resolution imager on NASA's Terra platform, Int. J. Remote Sens. 21 (5) (2000) 847–859.
[13] J.A. Sobrino, J.C. Jiménez-Muñoz, L. Paolini, Land surface temperature retrieval from Landsat TM 5, Remote Sens. Environ. 90 (4) (2004) 434–440.
[14] B. Zheng, S.W. Myint, C. Fan, Spatial configuration of anthropogenic land cover impacts on urban warming, Landsc. Urban Plan. 130 (2014) 104–111.

[15] P. Coseo, L. Larsen, How factors of land use/land cover, building configuration, and adjacent heat sources and sinks explain Urban Heat Islands in Chicago, Landsc. Urban Plan. 125 (2014) 117–129.

[16] S. Alavipanah, D. Haase, T. Lakes, S. Qureshi, Integrating the third dimension into the concept of urban ecosystem services: A review, Ecol. Indic. 72 (2017) 374–398.

[17] K. McGarigal, Landscape pattern metrics, Wiley StatsRef: Statistics Reference Online.

[18] W. Zhou, G. Huang, M.L. Cadenasso, Does spatial configuration matter? Understanding the effects of land cover pattern on land surface temperature in urban landscapes, Landsc. Urban Plan. 102 (1) (2011) 54–63.

[19] X. Li, W. Li, A. Middel, S. Harlan, A. Brazel, B. Turner Ii, Remote sensing of the surface urban heat island and land architecture in Phoenix, Arizona: Combined effects of land composition and configuration and cadastral–demographic–economic factors, Remote Sens. Environ. 174 (2016) 233–243.

[20] T.F. Stocker, D. Qin, G.-K. Plattner, M. Tignor, S.K. Allen, J. Boschung, A. Nauels, Y. Xia, V. Bex, P.M. Midgley, et al., Climate change 2013: The physical science basis, Contribution of Working Group I to the Fifth Assessment Report of the Intergovernmental Panel on Climate Change 1535, Cambridge university press, Cambridge New York, 2013.

[21] J. Niemelä, Is there a need for a theory of urban ecology? Urban Ecosyst. 3 (1) (1999) 57–65.

[22] A.A. Plowright, N.C. Coops, C.M. Chance, S.R. Sheppard, N.W. Aven, Multi-scale analysis of relationship between imperviousness and urban tree height using airborne remote sensing, Remote Sens. Environ. 194 (2017) 391–400.

[23] A.S. Fotheringham, Scale-independent spatial analysis, in: Accuracy of spatial databases, Taylor and Francis London, 1989, pp. 221–228.

[24] J. Song, S. Du, X. Feng, L. Guo, The relationships between landscape compositions and land surface temperature: Quantifying their resolution sensitivity with spatial regression models, Landsc. Urban Plan. 123 (2014) 145–157.

[25] M.G. Turner, Landscape ecology: the effect of pattern on process, Annu. Rev. Ecol. Syst. 20 (1) (1989) 171–197.

[26] W. Zhou, J. Wang, M.L. Cadenasso, Effects of the spatial configuration of trees on urban heat mitigation: A comparative study, Remote Sens. Environ. 195 (2017) 1–12.

[27] E. Johansson, R. Emmanuel, The influence of urban design on outdoor thermal comfort in the hot, humid city of Colombo, Sri Lanka, Int. J. Biometeorol. 51 (2) (2006) 119–133.

[28] M.A. Rahman, C. Hartmann, A. Moser-Reischl, M.F. von Strachwitz, H. Paeth, H. Pretzsch, S. Pauleit, T. Rötzer, Tree cooling effects and human thermal comfort under contrasting species and sites, Agricult. Forest Meteorol. 287 (2020) 107947.

[29] J. Konarska, B. Holmer, F. Lindberg, S. Thorsson, Influence of vegetation and building geometry on the spatial variations of air temperature and cooling rates in a high-latitude city, Int. J. Climatol. 36 (5) (2016) 2379–2395.

[30] Q. Yu, M. Acheampong, R. Pu, S.M. Landry, W. Ji, T. Dahigamuwa, Assessing effects of urban vegetation height on land surface temperature in the city of Tampa, Florida, USA, Int. J. Appl. Earth Obs. Geoinf. 73 (2018) 712–720.

[31] J. Chen, S. Jin, P. Du, Roles of horizontal and vertical tree canopy structure in mitigating daytime and nighttime urban heat island effects, Int. J. Appl. Earth Obs. Geoinf. 89 (2020) 102060.

[32] F. Sun, M. Liu, Y. Wang, H. Wang, Y. Che, The effects of 3D architectural patterns on the urban surface temperature at a neighborhood scale: Relative contributions and marginal effects, J. Cleaner Prod. 258 (2020) 120706.

[33] S. Alavipanah, J. Schreyer, D. Haase, T. Lakes, S. Qureshi, The effect of multi-dimensional indicators on urban thermal conditions, J. Cleaner Prod. 177 (2018) 115–123.

[34] X. Huang, Y. Wang, Investigating the effects of 3D urban morphology on the surface urban heat island effect in urban functional zones by using high-resolution remote sensing data: A case study of Wuhan, Central China, ISPRS J. Photogramm. Remote Sens. 152 (2019) 119–131.

[35] Y. Tian, W. Zhou, Y. Qian, Z. Zheng, J. Yan, The effect of urban 2D and 3D morphology on air temperature in residential neighborhoods, Lanc. Ecol., 1–18.

[36] F. Kong, H. Yin, C. Wang, G. Cavan, P. James, A satellite image-based analysis of factors contributing to the green-space cool island intensity on a city scale, Urban For. Urban Green. 13 (4) (2014) 846–853.

[37] X. Xu, Y. Zheng, J. Yin, R. Wu, Characteristics of high temperature and heat wave in Nanjing city and their impacts on human health, Chin. J. Ecol. 30 (12) (2011) 2815–2820.

[38] A. Gillespie, S. Rokugawa, T. Matsunaga, J.S. Cothern, S. Hook, A.B. Kahle, A temperature and emissivity separation algorithm for advanced spaceborne thermal emission and reflection radiometer (ASTER) images, IEEE Trans. Geosci. Remote Sens. 36 (4) (1998) 1113–1126.

[39] J. Chen, P. Du, C. Wu, J. Xia, J. Chanussot, Mapping urban land cover of a large area using multiple sensors multiple features, Remote Sens. 10 (6) (2018) 872.

[40] J. Li, C. Song, L. Cao, F. Zhu, X. Meng, J. Wu, Impacts of landscape structure on surface urban heat islands: A case study of Shanghai, China, Remote Sens. Environ. 115 (12) (2011) 3249–3263.

[41] Y. Chen, S. Yu, Impacts of urban landscape patterns on urban thermal variations in Guangzhou, China, Int. J. Appl. Earth Obs. Geoinf. 54 (2017) 65–71.

[42] A. Chen, L. Yao, R. Sun, L. Chen, How many metrics are required to identify the effects of the landscape pattern on land surface temperature? Ecol. Indic. 45 (2014) 424–433.

[43] K. McGarigal, FRAGSTATS: Spatial pattern analysis program for categorical maps. Computer software program produced by the authors at the University of Massachusetts, Amherst, 2002, http://www.umass.edu/landeco/research/fragstats/fragstats.html.

[44] I. Watson, G. Johnson, Graphical estimation of sky view-factors in urban environments, J. Climatol. 7 (2) (1987) 193–197.

[45] F. Lindberg, C.S.B. Grimmond, A. Gabey, B. Huang, C.W. Kent, T. Sun, N.E. Theeuwes, L. Järvi, H.C. Ward, I. Capel-Timms, et al., Urban multi-scale environmental predictor (UMEP): An integrated tool for city-based climate services, Environ. Model. Softw. 99 (2018) 70–87.

[46] W. Zhou, F. Cao, Effects of changing spatial extent on the relationship between urban forest patterns and land surface temperature, Ecol. Indic. 109 (2020) 105778.

[47] S. Peng, S. Piao, P. Ciais, R.B. Myneni, A. Chen, F. Chevallier, A.J. Dolman, I.A. Janssens, J. Penuelas, G. Zhang, et al., Asymmetric effects of daytime and night-time warming on northern hemisphere vegetation, Nature 501 (7465) (2013) 88.

[48] J. Bernard, M. Musy, I. Calmet, E. Bocher, P. Kéravec, Urban heat island temporal and spatial variations: Empirical modeling from geographical and meteorological data, Build. Environ. 125 (2017) 423–438.

[49] D.R. Seibold, R.D. McPHEE, Commonality analysis: A method for decomposing explained variance in multiple regression analyses, Hum. Commun. Res. 5 (4) (1979) 355–365.

[50] L.L. Nathans, F.L. Oswald, K. Nimon, Interpreting multiple linear regression: A guidebook of variable importance, Pract. Assess. Res. Eval. 17 (1) (2012) 9.

[51] F. Kong, H. Yin, P. James, L.R. Hutyra, H.S. He, Effects of spatial pattern of greenspace on urban cooling in a large metropolitan area of eastern China, Landsc. Urban Plan. 128 (2014) 35–47.

[52] E.A. Gage, D.J. Cooper, Urban forest structure and land cover composition effects on land surface temperature in a semi-arid suburban area, Urban For. Urban Green. 28 (2017) 28–35.

[53] J. Yan, W. Zhou, G.D. Jenerette, Testing an energy exchange and microclimate cooling hypothesis for the effect of vegetation configuration on urban heat, Agricult. Forest Meteorol. 279 (2019) 107666.

[54] H. Du, X. Song, H. Jiang, Z. Kan, Z. Wang, Y. Cai, Research on the cooling island effects of water body: A case study of Shanghai, China, Ecol. Indic. 67 (2016) 31–38.

[55] X. Sun, X. Tan, K. Chen, S. Song, X. Zhu, D. Hou, Quantifying landscape-metrics impacts on urban green-spaces and water-bodies cooling effect: The study of Nanjing, China, Urban For. Urban Green. (2020) 126838.

[56] S. Peng, Z. Feng, H. Liao, B. Huang, S. Peng, T. Zhou, Spatial-temporal pattern of, and driving forces for, urban heat island in China, Ecol. Indic. 96 (2019) 127–132.

[57] L. Zhao, X. Lee, R.B. Smith, K. Oleson, Strong contributions of local background climate to urban heat islands, Nature 511 (7508) (2014) 216–219.

[58] X. Yang, Y. Li, The impact of building density and building height heterogeneity on average urban albedo and street surface temperature, Build. Environ. 90 (2015) 146–156.

[59] G. Guo, X. Zhou, Z. Wu, R. Xiao, Y. Chen, Characterizing the impact of urban morphology heterogeneity on land surface temperature in Guangzhou, China, Environ. Model. Softw. 84 (2016) 427–439.

[60] H. Rezaei Rad, M. Rafieian, H. Sozer, Evaluating the effects of increasing of building height on land surface temperature, Int. J. Urban Manag. Energy Sustain. 1 (1) (2017) 11–16.

[61] A.K. Nassar, G.A. Blackburn, J.D. Whyatt, Dynamics and controls of urban heat sink and island phenomena in a desert city: Development of a local climate zone scheme using remotely-sensed inputs, Int. J. Appl. Earth Obs. Geoinf. 51 (2016) 76–90.

[62] X. Li, W. Zhou, Z. Ouyang, W. Xu, H. Zheng, Spatial pattern of greenspace affects land surface temperature: evidence from the heavily urbanized Beijing metropolitan area, China, Lanc. Ecol. 27 (6) (2012) 887–898.

[63] A. Buyantuyev, J. Wu, Urban heat islands and landscape heterogeneity: linking spatiotemporal variations in surface temperatures to land-cover and socioeconomic patterns, Lanc. Ecol. 25 (1) (2010) 17–33.